Supplementary information

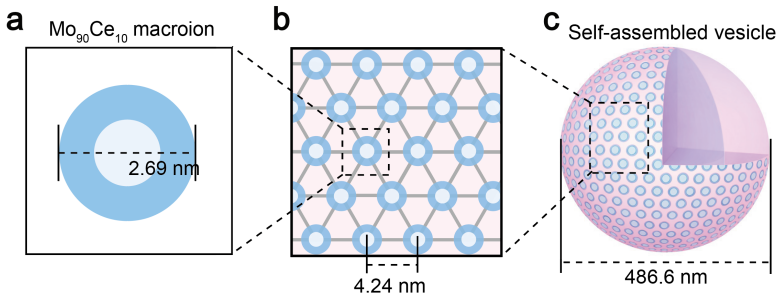

Supplementary Fig. 1 | Structural organization of $Mo_{90}Ce_{10}$ macroions in their self-assembled vesicles. a, $Mo_{90}Ce_{10}$ is stably dispersed in aqueous solution as intact macroionic units, with a diameter of ~2.69 nm. **b**, A magnified schematic of the self-assembled vesicle surface shows a highly ordered hexagonal packing of $Mo_{90}Ce_{10}$ macroions, with a center-to-center spacing of ~4.24 nm. **c,** $Mo_{90}Ce_{10}$ macroions undergo reversible self-assembly to form hollow, blackberry-like vesicular nanoclusters with an overall diameter of ~486.6 nm.

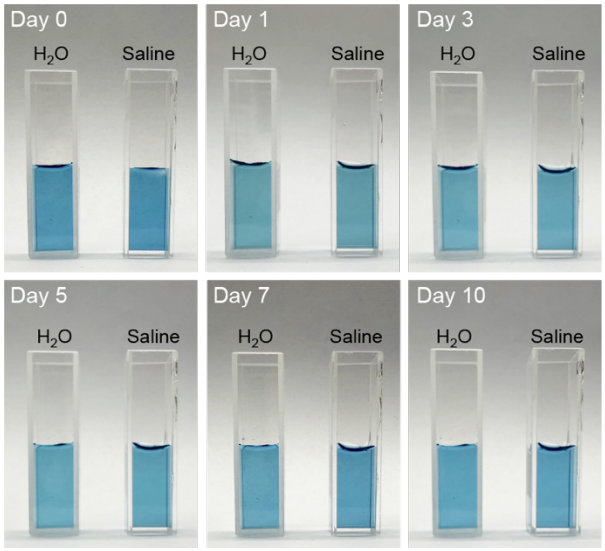

Supplementary Fig. 2 | $Mo_{90}Ce_{10}$ remains stable in solution in both water and normal saline. Digital photos of $Mo_{90}Ce_{10}$ dispersions in water and normal saline at different time points.

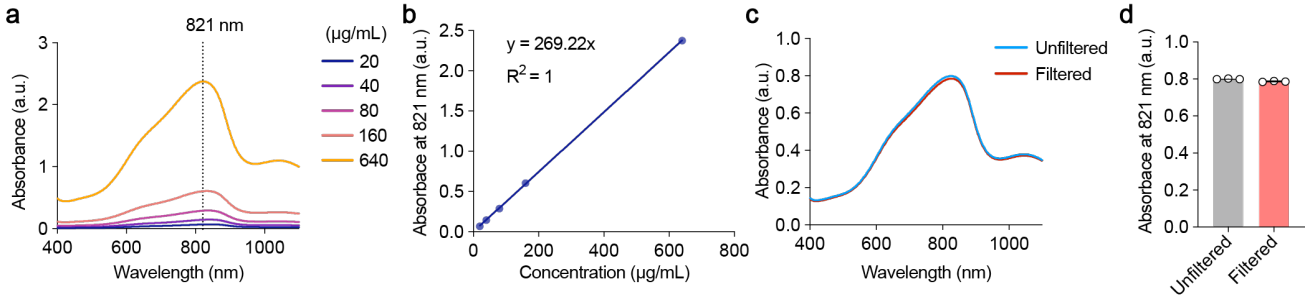

Supplementary Fig. 3 | $Mo_{90}Ce_{10}$ solution maintains its UV–Vis absorbance profile after 0.22 μm filtration. **a**, UV-Vis spectra of $Mo_{90}Ce_{10}$ aqueous solution at different concentrations. **b**, Concentration-absorbance relationship and linear regression at the absorption peak (821 nm). **c**, UV-Vis spectra of $Mo_{90}Ce_{10}$ solution before and after 0.22 μm filtration. **d**, Absorbance values at 821 nm for the $Mo_{90}Ce_{10}$ solution before and after 0.22 μm filtration (n = 3). Absorbance is presented in a.u. (arbitrary units). *P* values were determined by unpaired, two-tailed Student's t-test (**d**). Data are presented as mean ± s.e.m. Source data are provided as a Source Data file.

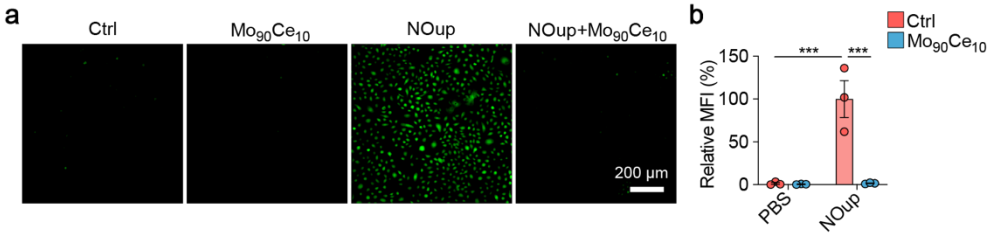

Supplementary Fig. 4 | $Mo_{90}Ce_{10}$ reduces RNS levels in keratinocytes. a,**b**, Representative images of intracellular RNS signals in HaCaT cells after treatment with NOup or $Mo_{90}Ce_{10}$ (**a**) and quantification of mean fluorescence intensity (MFI) (n = 3) (**b**). Scale bar, 200 μm. HaCaT cells, human immortalized keratinocytes; RNS, reactive nitrogen species. *** $P < 0.001$. *P* values were determined by two-way ANOVA (**b**). All tests were two-sided, and multiple comparisons were corrected as appropriate. Data are presented as mean ± s.e.m. Source data are provided as a Source Data file.

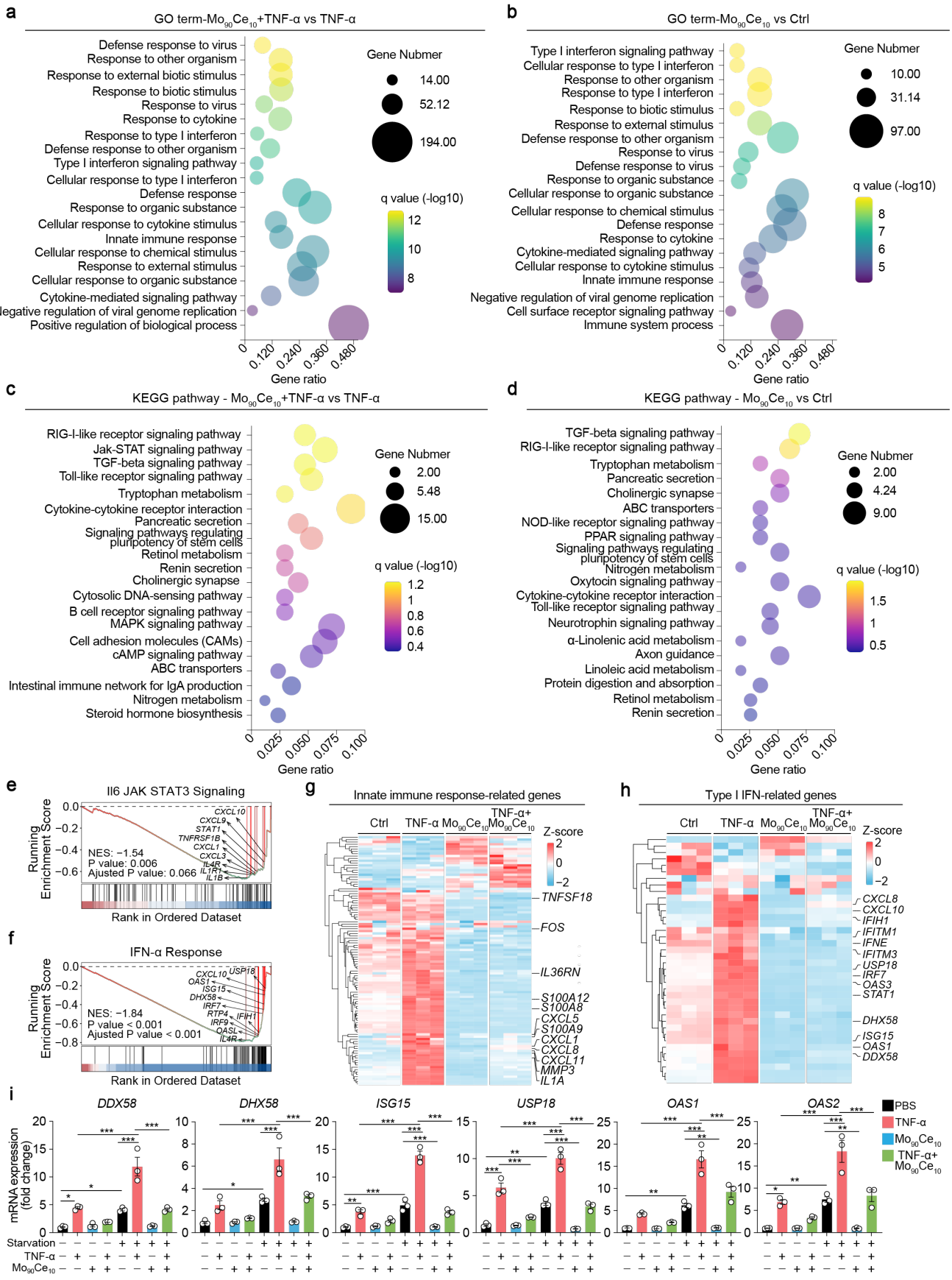

Supplementary Fig. 5 | $Mo_{90}Ce_{10}$ downregulates genes involved in the innate immune response and type I IFN signaling in keratinocytes. a,**b**, Enrichment of the top 20 GO terms of DEGs in HaCaT cells treated

with PBS or $Mo_{90}Ce_{10}$ and stimulated with (**a**) or without (**b**) 50 ng/mL TNF-α for 6 h. **c**,**d**, Enrichment of the top 20 KEGG pathways of DEGs in HaCaT cells treated with PBS or $Mo_{90}Ce_{10}$ and stimulated with (**c**) or without (**d**) 50 ng/mL TNF-α for 6 h. **e**,**f**, GSEA of the indicated pathways showing a significant downregulation after treatment with $Mo_{90}Ce_{10}$ under 50 ng/mL TNF-α stimulation for 6 h. **g,h**, Heatmap of the expression of selected genes involved in innate immune response (**g**) or type I IFN signaling pathway (**h**) based on GO terms and KEGG analysis. **i**, Quantification of genes related to the type I IFN signaling pathway by RT-qPCR after the indicated treatments (n = 3). GO, Gene Ontology; DEGs, differentially expressed genes; KEGG, Kyoto Encyclopedia of Genes and Genomes; HaCaT cells, human immortalized keratinocytes; IFN, interferon. * $P < 0.05$, ** $P < 0.01$, *** $P < 0.001$. P values were determined by one-way ANOVA (**i**). All tests were two-sided, and multiple comparisons were corrected as appropriate. Data are presented as mean ± s.e.m. Source data are provided as a Source Data file.

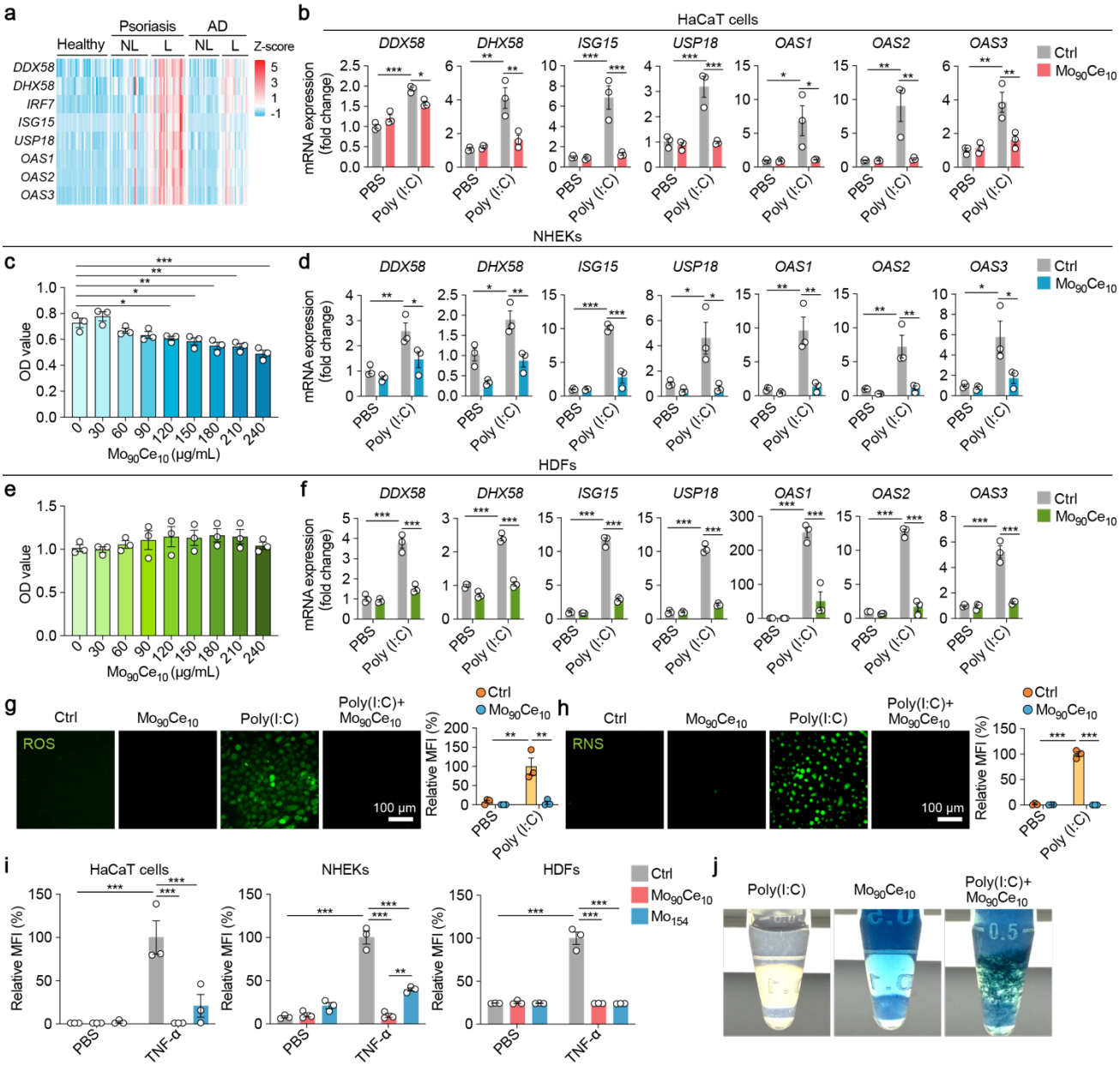

Supplementary Fig. 6 | $Mo_{90}Ce_{10}$ mitigates dsRNA-induced inflammatory responses and the concomitant elevation of intracellular ROS and RNS. a, Heatmap of dsRNA-related gene expression analyzed from publicly available (GEO database, accession No. GSE121212) RNA-seq analysis of healthy controls (n = 38) and patients with psoriasis (n = 28) or AD (n = 27). **b**, Quantification of dsRNA-related genes in HaCaT cells by RT-qPCR after treatment with 90 μg/mL $Mo_{90}Ce_{10}$ or PBS with or without poly(I:C) stimulation (n = 3). **c**, CCK-8 assay showing cell viability of NHEKs after treatment with different concentrations of $Mo_{90}Ce_{10}$ (n = 3). **d**, Quantification of dsRNA-related genes in NHEKs by RT-qPCR after treatment with $Mo_{90}Ce_{10}$ or PBS with or without poly(I:C) stimulation (n = 3). **e**, CCK-8 assay showing cell viability of HDFs after treatment with different concentrations of $Mo_{90}Ce_{10}$ (n = 3). **f**, Quantification of dsRNA-related genes in HDFs by RT-qPCR after treatment with $Mo_{90}Ce_{10}$ or PBS with or without poly(I:C) stimulation (n = 3). **g**,**h**, Representative images of intracellular ROS (**g**) or RNS (**h**) levels in HaCaT cells after treatment with poly(I:C), $Mo_{90}Ce_{10}$ or their combination, and quantification of MFI (n = 3). **i**, Relative MFI of J2 staining in the indicated groups in **Fig. 2i**, **k** or **m** (n = 3). **j**, Representative images of poly(I:C), $Mo_{90}Ce_{10}$ and their combination in aqueous solution. Scale bars, 100 μm (**g** and **i**). AD, atopic dermatitis; NL, non-lesional skin; L, lesional skin; HaCaT

cells, human immortalized keratinocytes; NHEKs, normal human epidermal keratinocytes; HDFs, human dermal fibroblasts; Poly(I:C), polyriboinosinic acid-polyribocytidylic acid; ROS, reactive oxygen species; RNS, reactive nitrogen species; MFI, mean fluorescence intensity. * $P < 0.05$, ** $P < 0.01$, *** $P < 0.001$. P values were determined by two-way ANOVA (**b**, **d**, **f** and **g–i**) and one-way ANOVA (**c** and **e**). All tests were two-sided, and multiple comparisons were corrected as appropriate. Data are presented as mean ± s.e.m. Source data are provided as a Source Data file.

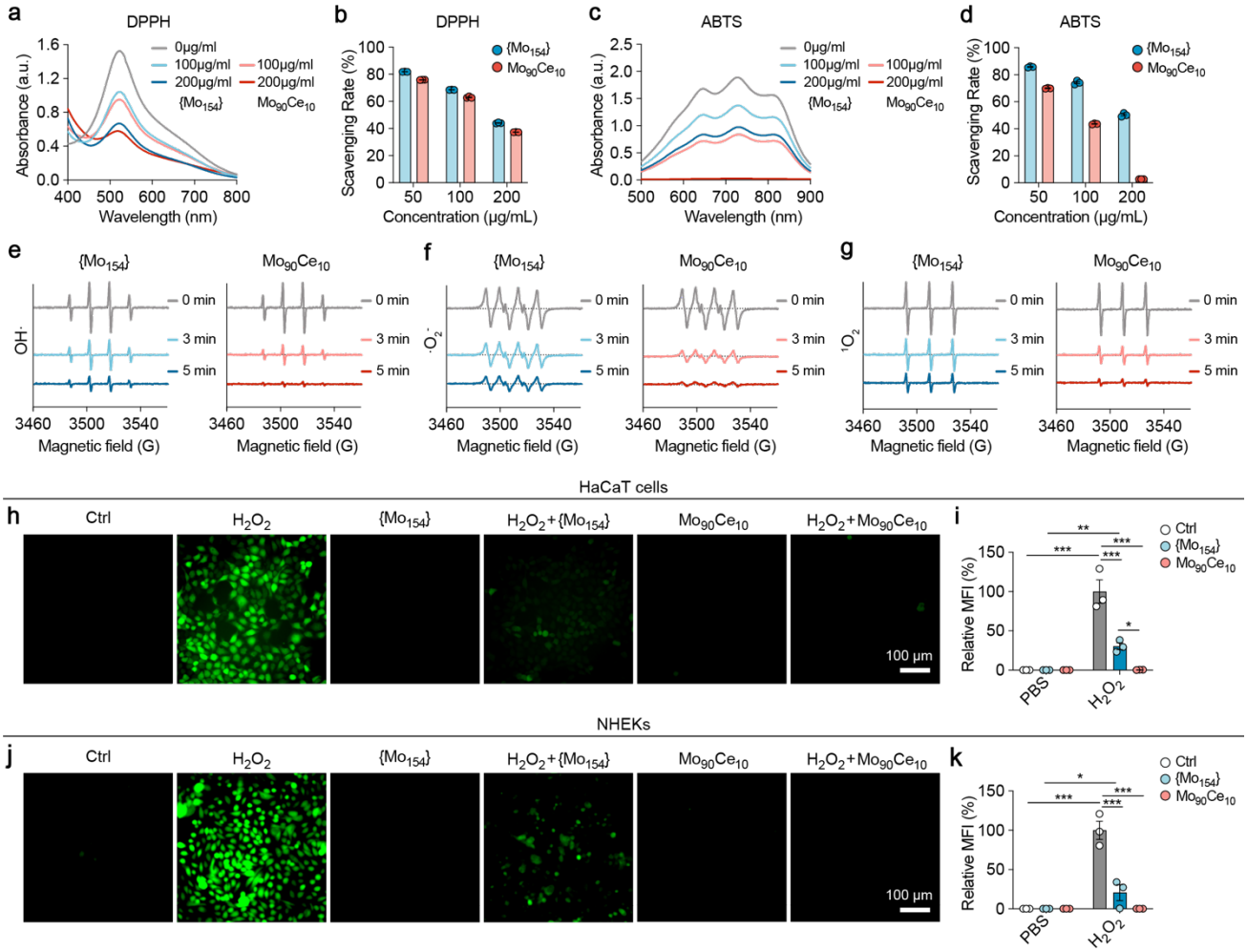

Supplementary Fig. 7 | $Mo_{90}Ce_{10}$ shows stronger free radical–scavenging activity and exhibits a more potent suppression of intracellular ROS than {Mo_{154}}. a,b, UV–Vis spectra of DPPH radicals after reaction with $Mo_{90}Ce_{10}$ or {Mo_{154}} at various concentrations (**a**), and the corresponding quantification (**b**). Absorbance is presented in a.u. (arbitrary units). **c,d,** UV–Vis spectra of ABTS radicals after reaction with $Mo_{90}Ce_{10}$ or {Mo_{154}} at various concentrations (**c**), along with the corresponding quantification (**d**). Absorbance is presented in a.u. (arbitrary units). **e–g**, ESR spectra of different free radicals—including hydroxyl radicals (·OH) (**e**), superoxide anions ($O_2^{-}\cdot$) (**f**), and singlet oxygen ($^1O_2$) (**g**)—after reaction with $Mo_{90}Ce_{10}$ or {Mo_{154}} at the indicated concentrations. **h**,**i**, Representative images (**h**) and their quantification (**i**) of intracellular ROS levels (green) in HaCaT cells using the DCFH-DA probe (n = 3). **j**,**k**, Representative images (**j**) and their quantification (**k**) of intracellular ROS levels (green) in NHEKs using the DCFH-DA probe (n = 3). Scale bars, 100 μm (**h** and **j**). HaCaT cells, human immortalized keratinocytes; NHEKs, normal human epidermal keratinocytes; MFI, mean fluorescence intensity. * $P < 0.05$, ** $P < 0.01$, *** $P < 0.001$. P values were determined by two-way ANOVA (**i** and **k**). All tests were two-sided, and multiple comparisons were corrected as appropriate. Data are presented as mean ± s.e.m. Source data are provided as a Source Data file.

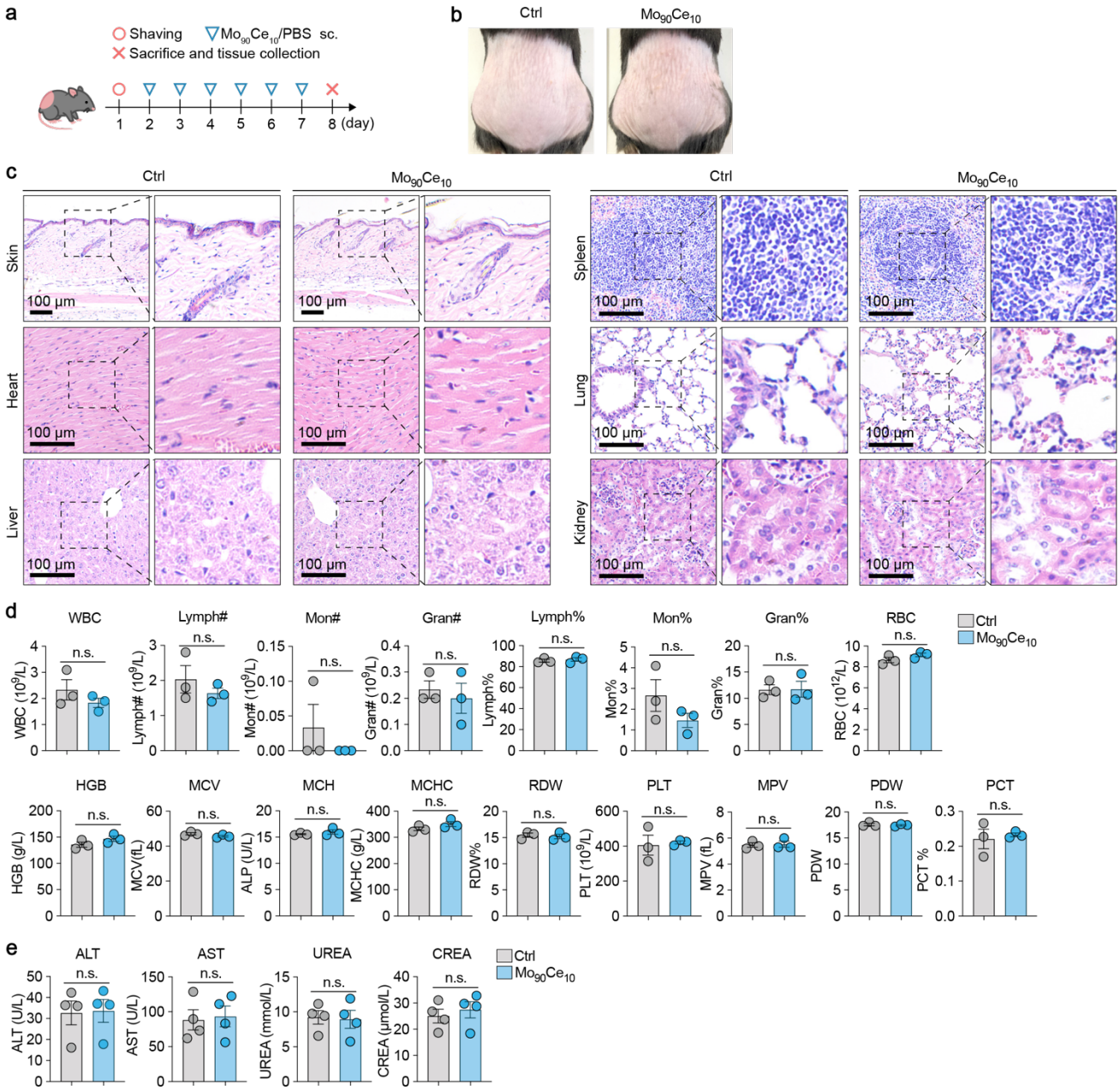

Supplementary Fig. 8 | Short-term in vivo biosafety evaluation of $Mo_{90}Ce_{10}$ treatment. a, Schematic illustration of biosafety evaluation of topical treatment with $Mo_{90}Ce_{10}$ or PBS. **b**, Representative skin morphology of mice after treatment with $Mo_{90}Ce_{10}$ or PBS at the indicated times. **c**, Representative H&E-stained sections of skin, heart, liver, spleen, lungs, and kidneys for histopathological evaluation of the indicated groups in vivo. Scale bars, 100 μm. **d**,**e**, Complete blood count (n = 3) (**d**) and blood biochemical analysis (n = 4) (**e**) after treatment with $Mo_{90}Ce_{10}$ or PBS. WBC, white blood cell count; Lymph#, lymphocyte count; Mon#, monocyte count; Gran#, granulocyte count; Lymph%, lymphocyte ratio; Mon%, monocyte ratio; Gran%, granulocyte ratio; RBC, red blood cell count; HGB, hemoglobin; MCV, mean corpuscular volume; MCH, mean corpuscular hemoglobin; MCHC, mean corpuscular hemoglobin concentration; RDW, red cell distribution width; PLT, platelet count; MPV, mean platelet volume; PDW, platelet distribution width; PCT, thrombocytocrit; ALT, alanine aminotransferase; AST, aspartate aminotransferase; CREA, creatinine; ALP, alkaline phosphatase; n.s., not significant. *P* values were determined by unpaired, two-tailed Student's t-test (**d** and **e**). Data are presented as mean ± s.e.m. Source data are provided as a Source Data file.

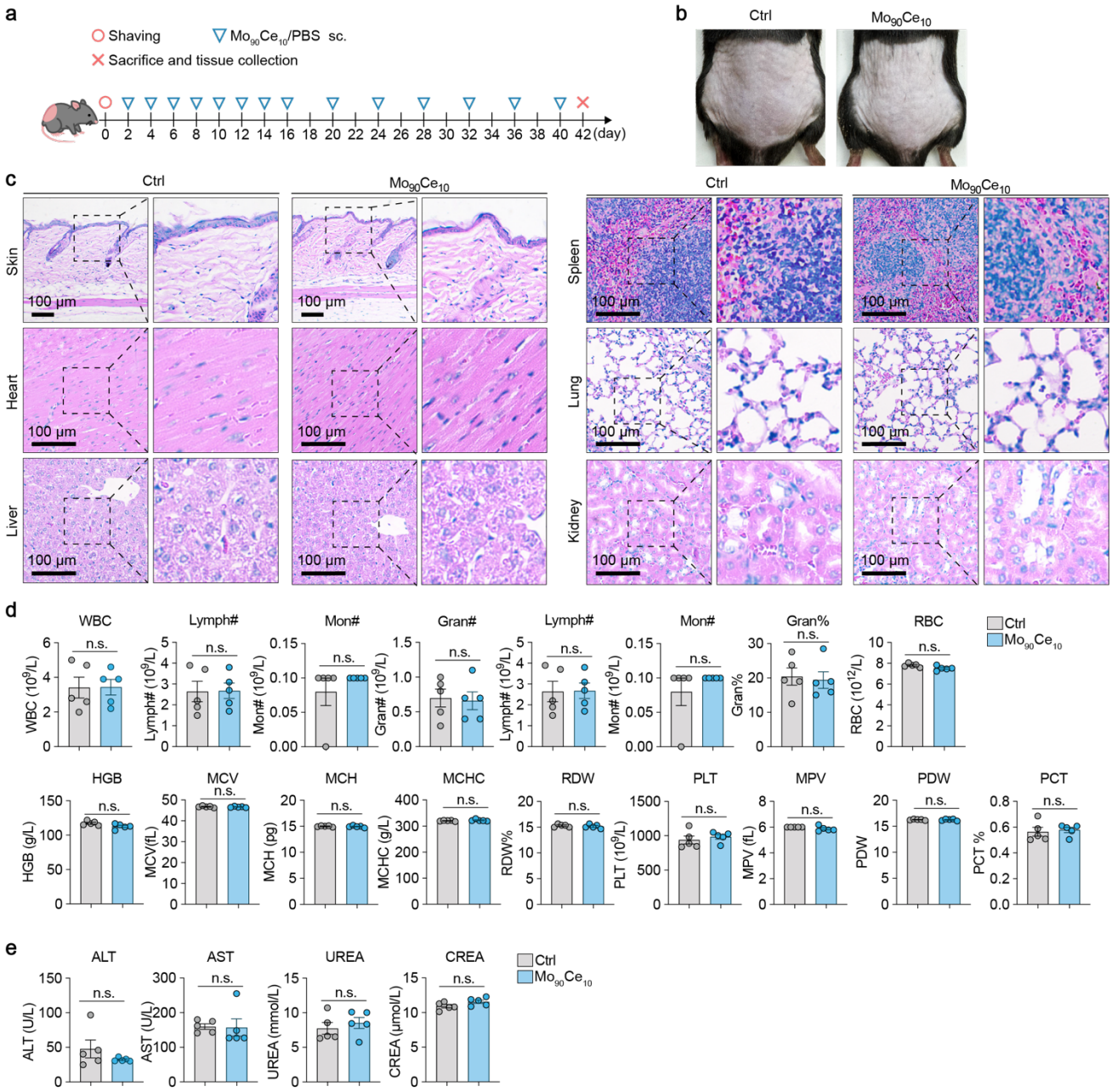

Supplementary Fig. 9 | Long-term in vivo biosafety evaluation of $Mo_{90}Ce_{10}$ treatment. a, Schematic illustration of biosafety evaluation of the topical treatment with $Mo_{90}Ce_{10}$ or PBS. **b**, Representative skin morphology of mice after treatment with $Mo_{90}Ce_{10}$ or PBS at the indicated times. **c**, Representative H&E-stained sections of skin, heart, liver, spleen, lungs, and kidneys for histopathological evaluation of the indicated groups in vivo. Scale bars, 100 μm. **d**,**e**, Complete blood count (**d**) and blood biochemical analysis (**e**) after treatment with $Mo_{90}Ce_{10}$ or PBS (n = 5). WBC, white blood cell count; Lymph#, lymphocyte count; Mon#, monocyte count; Gran#, granulocyte count; Lymph%, lymphocyte ratio; Mon%, monocyte ratio; Gran%, granulocyte ratio; RBC, red blood cell count; HGB, hemoglobin; MCV, mean corpuscular volume; MCH, mean corpuscular hemoglobin; MCHC, mean corpuscular hemoglobin concentration; RDW, red cell distribution width; PLT, platelet count; MPV, mean platelet volume; PDW, platelet distribution width; PCT, thrombocytocrit; ALT, alanine aminotransferase; AST, aspartate aminotransferase; CREA, creatinine; ALP, alkaline phosphatase; n.s., not significant. * $P < 0.05$. P values were determined by unpaired, two-tailed Student's t-test (**d** and **e**). Data are presented as mean ± s.e.m. Source data are provided as a Source Data file.

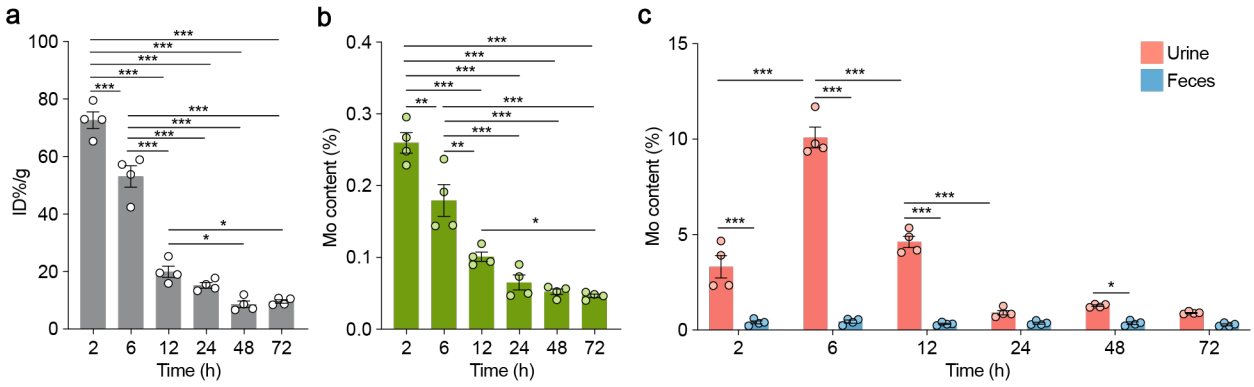

Supplementary Fig. 10 | Local retention, systemic circulation and excretion after $Mo_{90}Ce_{10}$ administration. **a**, Mo distribution in murine skin at the indicated time points after subcutaneous injection of $Mo_{90}Ce_{10}$ (n = 4). **b,c**, Mo concentrations in blood (**b**) and in urine and feces (**c**) collected from mice at the indicated time points after subcutaneous injection of $Mo_{90}Ce_{10}$ (n = 4). * $P < 0.05$, ** $P < 0.01$, *** $P < 0.001$. P values were determined by one-way ANOVA (**a** and **b**) or two-way ANOVA (**c**). All tests were two-sided, and multiple comparisons were corrected as appropriate. Data are presented as mean ± s.e.m. Source data are provided as a Source Data file.

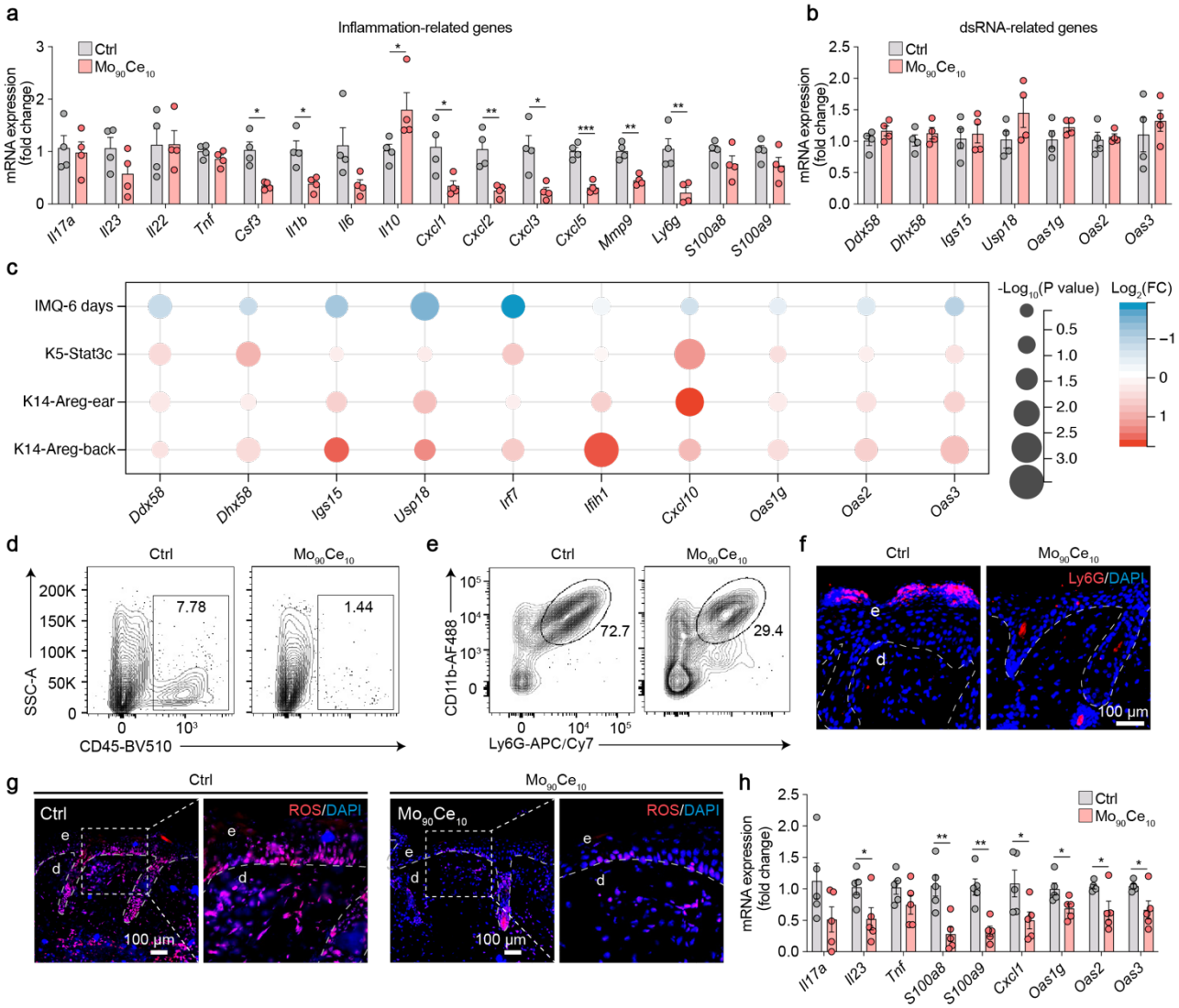

Supplementary Fig. 11 | $Mo_{90}Ce_{10}$ treatment attenuates psoriasis-like skin inflammation, related to Fig. 4. a,**b**, RT-qPCR analysis of inflammation-related genes (**a**) and dsRNA-related genes (**b**) in dorsal skin of mice treated with $Mo_{90}Ce_{10}$ or PBS after 6 days of IMQ treatment, related to **Fig. 4f**. **c**, Dot plot of dsRNA-related gene expression from publicly available (GEO database, accession No. GSE27628) RNA-seq analysis of psoriasis-like mouse models compared with control mice. **d**,**e**, Flow cytometry analysis of $CD45^+$ cells (**d**) or neutrophils (**e**) in IMQ-induced psoriasis-like skin lesions. **f**, Immunofluorescence analysis of $Ly6G^+$ cells in IMQ-induced lesional skin from mice treated with $Mo_{90}Ce_{10}$ or PBS. **g**, Representative fluorescence images showing ROS levels in skin lesions of IMQ-treated mice after 6 days, detected by dihydroethidium (DHE) staining (timeline consistent with **Fig. 4l**). **h**, RT-qPCR analysis of inflammation-related genes and dsRNA-related genes in ear skin of mice treated with $Mo_{90}Ce_{10}$ or PBS after IL-23 induction, related to **Fig. 4r** (n = 5). IMQ, imiquimod; dsRNA, double-stranded RNA; FC, fold change; ROS, reactive oxygen species; e, epidermis; d, dermis. Scale bars, 100 μm. * $P < 0.05$, ** $P < 0.01$, *** $P < 0.001$. P values were determined by unpaired, two-tailed Student's t-test (**a**, **b** and **h**). Data are presented as mean ± s.e.m. Source data are provided as a Source Data file.

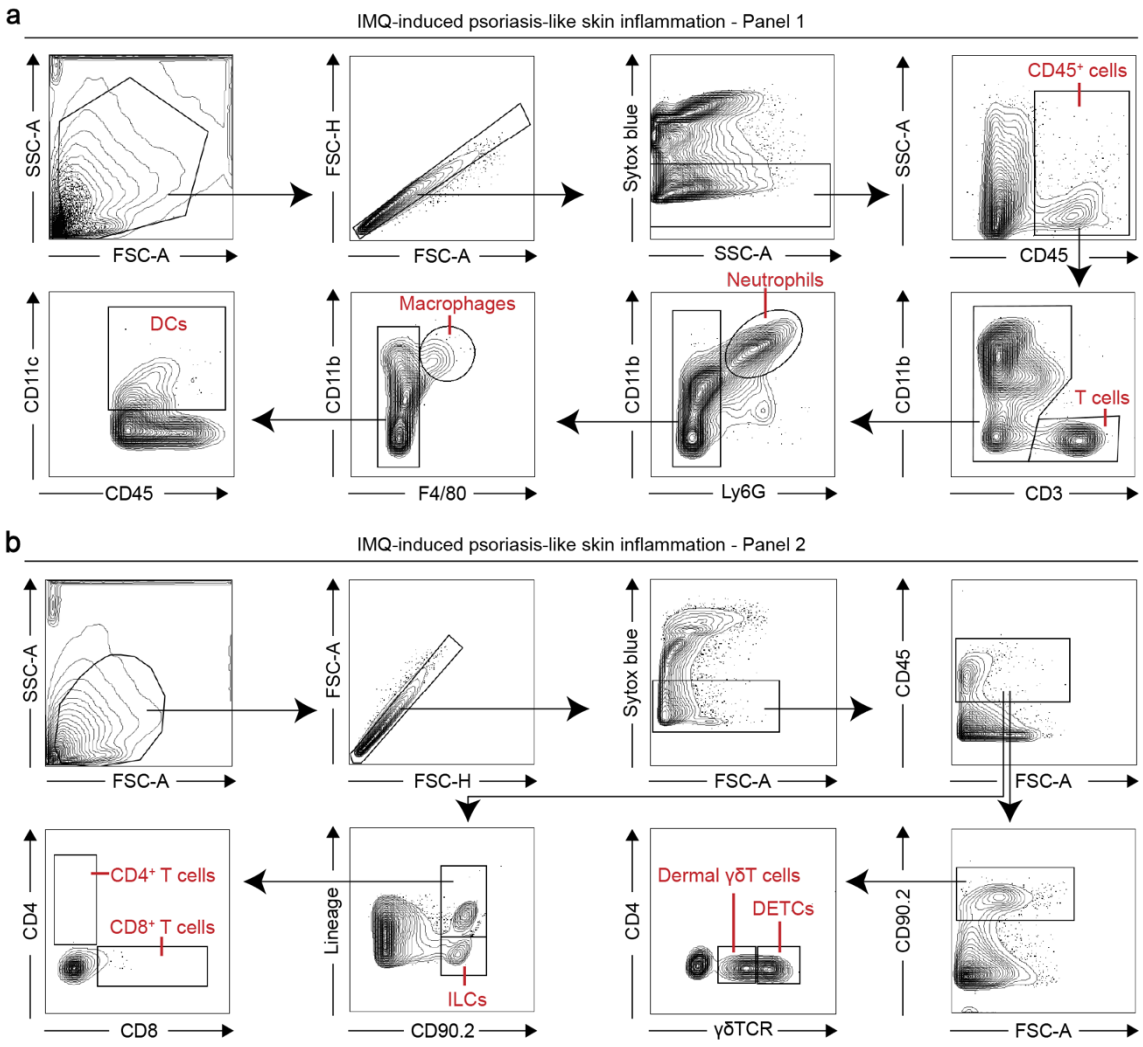

Supplementary Fig. 12 | Selected flow cytometry gating strategies for evaluating immune cell infiltration in IMQ-induced psoriasis-like skin lesions. a,**b**, Different cell subsets were identified using distinct antibody cocktails in IMQ-induced psoriasis-like skin lesions. The skin-infiltrating immune cells were analyzed by flow cytometry to identify $CD45^+$ cells (**a**), T cells (**a**), neutrophils (**a**), macrophages (**a**), DCs (**a**), dermal γδT cells (**b**), DETCs (**b**), ILCs (**b**), $CD4^+$ T cells (**b**), and $CD8^+$ T cells (**b**) in skin lesions. DCs, dendritic cells; ILCs, innate lymphoid cells.

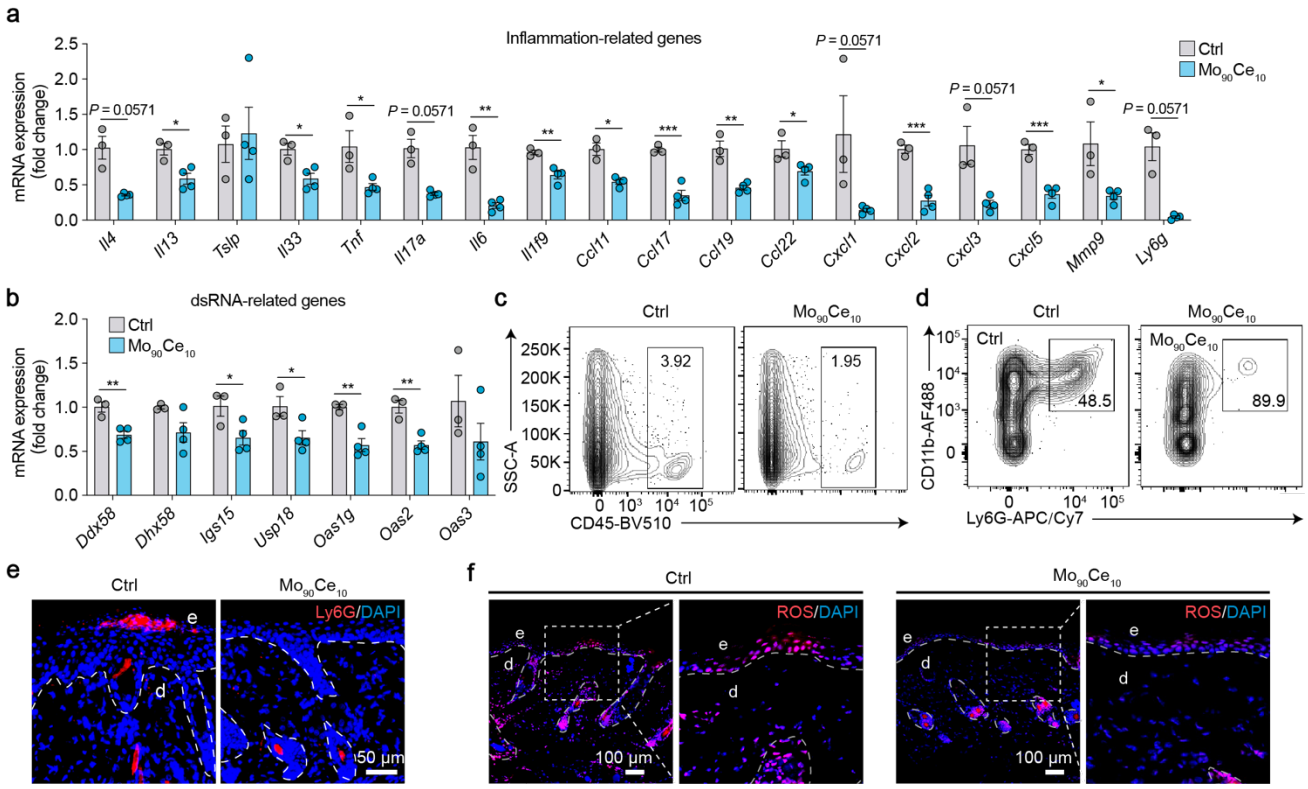

Supplementary Fig. 13 | $Mo_{90}Ce_{10}$ treatment alleviates AD-like skin inflammation, related to Fig. 5. a,**b**, RT-qPCR analysis of inflammation-related genes (**a**) and dsRNA-related genes (**b**) in dorsal skin of mice treated with $Mo_{90}Ce_{10}$ or PBS after 6 days of MC903 treatment, related to **Fig. 5f**. **c**,**d**, Flow cytometry analysis of $CD45^+$ cells (**c**) or neutrophils (**d**) in MC903-induced AD-like skin lesions. **e**, Immunofluorescence analysis of $Ly6G^+$ cells in MC903-induced lesional skin from mice treated with $Mo_{90}Ce_{10}$ or PBS. **f**, Representative fluorescence images showing ROS levels in skin lesions of MC903-treated mice after 6 days, detected by dihydroethidium (DHE) staining (timeline consistent with **Fig. 5j**). n = 3 mice in the control group and n = 4 mice in the $Mo_{90}Ce_{10}$-treated group. Scale bars, 50 μm (**e** and **f**). dsRNA, double-stranded RNA; FC, fold change; AD, atopic dermatitis. * $P < 0.05$, ** $P < 0.01$, *** $P < 0.001$. P values were determined by unpaired, two-tailed Student's t-test (**a** and **b**). Data are presented as mean ± s.e.m. Source data are provided as a Source Data file.

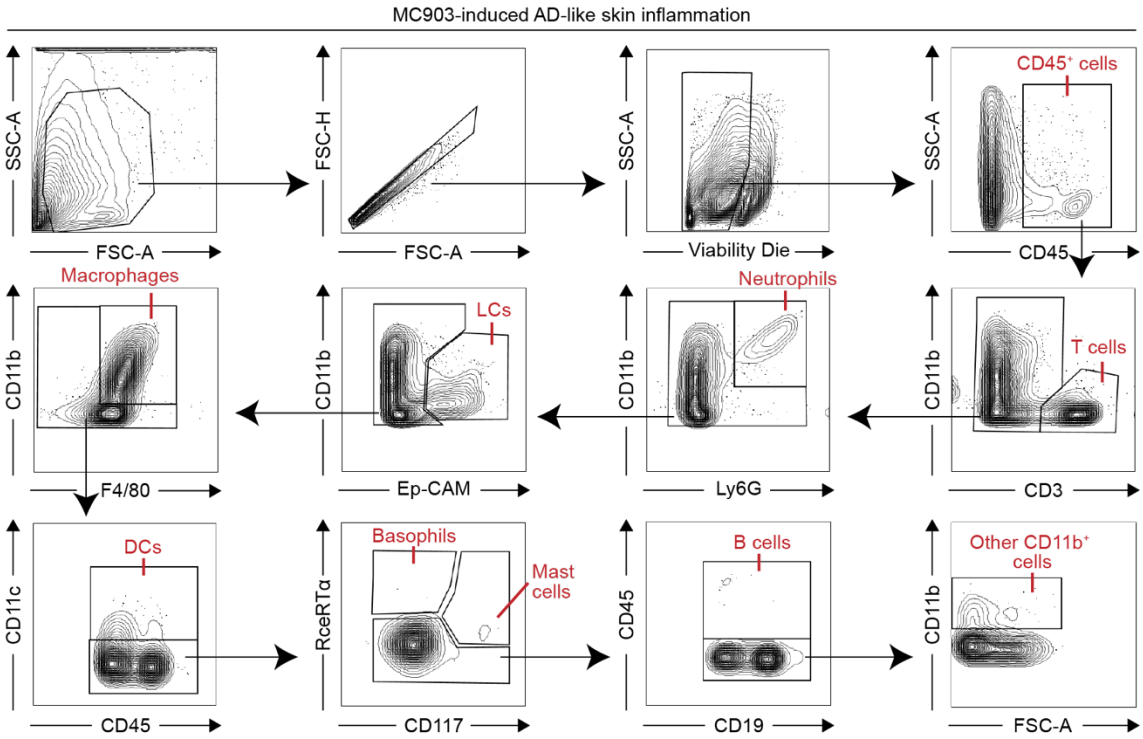

Supplementary Fig. 14 | Selected flow cytometry gating strategies for evaluating immune cell infiltration in MC903-induced AD-like skin lesions. Different cell subsets were identified using distinct antibody cocktails in MC903-induced AD-like skin lesions. The skin-infiltrating immune cells were analyzed by flow cytometry to identify $CD45^+$ cells, T cells, neutrophils, LCs, macrophages, DCs, basophils, mast cells, B cells, and other $CD11b^+$ cells. AD, atopic dermatitis. LCs, Langerhans cells; DCs, dendritic cells.

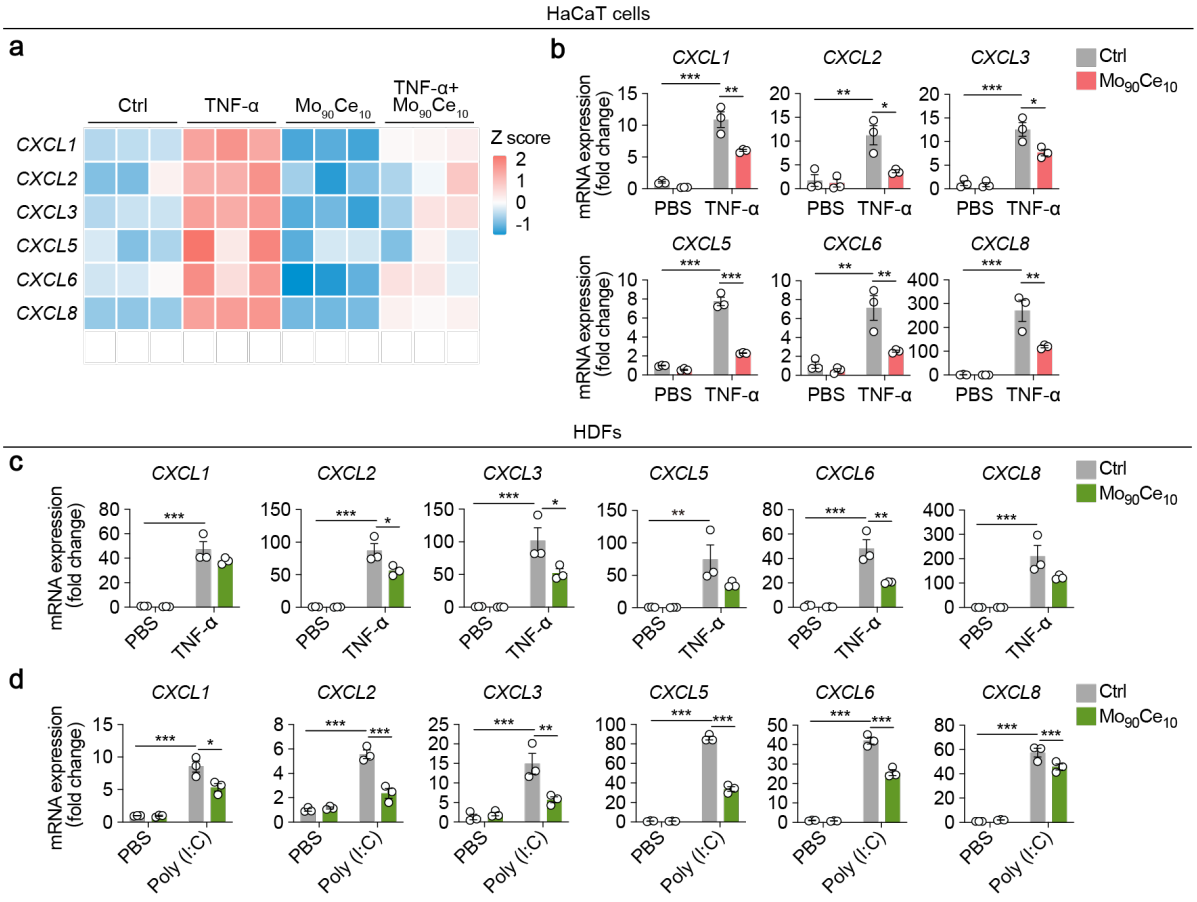

Supplementary Fig. 15 | $Mo_{90}Ce_{10}$ treatment markedly decreases the expression of neutrophil chemotaxis-related genes in human keratinocytes and dermal fibroblasts. a, Heatmap showing z-scores of neutrophil chemotaxis-related gene expression assessed by RNA-seq as described in **Fig. 2a**. **b**,**c**, Quantification of neutrophil chemotaxis-related genes in HaCaT cells (**b**) or HDFs (**c**) via RT-qPCR after treatment with $Mo_{90}Ce_{10}$ or PBS, with or without TNF-α stimulation (n = 3). **d**, Quantification of neutrophil chemotaxis-related genes in HDFs via RT-qPCR after treatment with $Mo_{90}Ce_{10}$ or PBS, with or without poly(I:C) stimulation (n = 3). HaCaT cells, human immortalized keratinocytes; HDFs, human dermal fibroblasts; Poly(I:C), polyriboinosinic acid-polyribocytidylic acid. * $P < 0.05$, ** $P < 0.01$, *** $P < 0.001$. P values were determined by two-way ANOVA (**b**–**d**). All tests were two-sided, and multiple comparisons were corrected as appropriate. Data are presented as mean ± s.e.m. Source data are provided as a Source Data file.

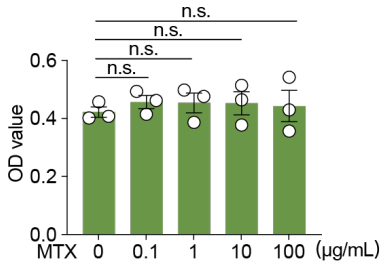

Supplementary Fig. 16 | MTX concentration-dependent cytotoxicity in HaCaT cells. CCK-8 assay showing HaCaT cell viability after treatment with different concentrations of MTX (n = 3). MTX, methotrexate.n.s., not significant. *P* values were determined by one-way ANOVA. All tests were two-sided, and multiple comparisons were corrected as appropriate. Data are presented as mean ± s.e.m. Source data are provided as a Source Data file.

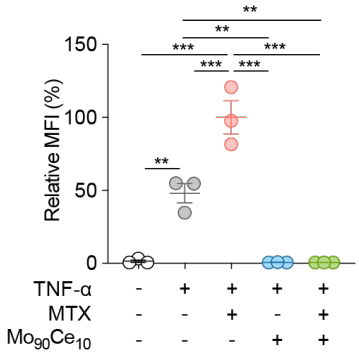

Supplementary Fig. 17 | $Mo_{90}Ce_{10}$ alleviates MTX-induced dsRNA accumulation. Quantification of the relative MFI of dsRNA-specific antibody J2 staining in HaCaT cells treated with MTX, $Mo_{90}Ce_{10}$ or their combination with or without TNF-α for 6 h, assessed by immunocytochemistry (n = 3). dsRNA, double-stranded RNA; MTX, methotrexate; MFI, mean fluorescence intensity. ** $P < 0.01$, *** $P < 0.001$. *P* values were determined by one-way ANOVA. All tests were two-sided, and multiple comparisons were corrected as appropriate. Data are presented as mean ± s.e.m. Source data are provided as a Source Data file.

Supplementary Table 1. Primers for RT-qPCR

Gene	Sequence of forward primer (5'→3')	Sequence of reverse primer (5'→3')
hCXCL1	CAATCCTGCATCCCCCATAGT	GGATTTGTCACTGTTCAGCATCTT
hCXCL2	AGATCAATGTGACGGCAGGG	TCTCTGCTCTAACACAGAGGGA
hCXCL3	AAAAGATACTGAACAAGGGGAGCA	CTCTGGTAAGGGCAGGGACC
hCXCL5	AGCTGCGTTGCGTTTGTTTAC	TGGCGAACACTTGCAGATTAC
hCXCL6	AGAGCTGCGTTGCACTTGTT	GCAGTTTACCAATCGTTTTGGGG
hCXCL8	AACTGAGAGTGATTGAGAGTGG	ATGAATTCTCAGCCCTCTTCAA
hCXCL10	GTGGCATTCAAGGAGTACCTC	TGATGGCCTTCGATTCTGGATT
hIL36G	GCCGTCTATCAATCAATGTG	GCTGTTCTCCAACCTTCTC
hIL6	ACTCACCTCTTCAGAACGAATTG	CCATCTTTGGAAGGTTCAGGTTG
hDDX58	TGTGCTCCTACAGGTTGTGGA	CACTGGGATCTGATTCGCAAAA
hDHX58	GGGCCTCCAAACTCGATGG	TTCTGGGGTGACATGATGCAC
hISG15	CGCAGATCACCCAGAAGATCG	TTCGTCGCATTTGTCCACCA
hIFIH1	TCGAATGGGTATTCCACAGACG	GTGGCGACTGTCCTCTGAA
hIFNE	GGCCTCTACCACTATCTTCTCTC	ACACTGCTGAATTGACAAGGTTT
hIRF7	GCTGGACGTGACCATCATGTA	GGGCCGTATAGGAACGTGC
hOAS1	TGTCCAAGGTGGTAAAGGGTG	CCGGCGATTTAACTGATCCTG
hOAS2	CTCAGAAGCTGGGTTGGTTTAT	ACCATCTCGTCGATCAGTGTC
hOAS3	GAAGGAGTTCGTAGAGAAGGCG	CCCTTGACAGTTTTCAGCACC
hUSP18	AACGTGCCCTTGTTTGTCCAA	GAGTCCTTCACCCGGATCGTA
hGAPDH	GGAGCGAGATCCCTCCAAAAT	GGCTGTTGTCATACTTCTCATGG
mIL17a	TTTAACTCCCTTGGCGCAAAA	CTTTCCCTCCGCATTGACAC
mIl23	ACCTGCTTGACTCTGACA	CCACTGCTGACTAGAACTC
mIl22	ACCTGCTTGACTCTGACA	CCACTGCTGACTAGAACTC
mTnf	CTGAACTTCGGGGTGATCGG	GGCTTGTCACTCGAATTTTGAGA
mCsf3	ATGGCTCAACTTTCTGCCCAG	CTGACAGTGACCAGGGGAAC
mIl1b	GCAACTGTTCCTGAACTCAACT	ATCTTTTGGGGTCCGTCAACT
mIl6	TAGTCCTTCCTACCCCAATTTCC	TTGGTCCTTAGCCACTCCTTC
mIl10	GCTCTTACTGACTGGCATGAG	CGCAGCTCTAGGAGCATGTG
mCxcl1	CTGGGATTCACCTCAAGAACATC	CAGGGTCAAGGCAAGCCTC
mCxcl2	CCAACCACCAGGCTACAGG	GCGTCACACTCAAGCTCTG
mCxcl3	CCAGACAGAAGTCATAGCCAC	CTTCATCATGGTGAGGGGCTT
mCxcl5	GTTCCATCTCGCCATTCATGC	GCGGCTATGACTGAGGAAGG
mMmp9	CTGGACAGCCAGACACTAAAG	CTCGCGGCAAGTCTTCAGAG
mLy6g	GACTTCCTGCAACACAACTACC	ACAGCATTACCAGTGATCTCAGT
mS100a8	AAATCACCATGCCCTCTACAAG	CCCACTTTTATCACCATCGCAA
mS100a9	ATACTCTAGGAAGGAAGGACACC	TCCATGATGTCATTTATGAGGGC

mDdx58	AAGAGCCAGAGTGTCAGAATCT	AGCTCCAGTTGGTAATTTCTTGG
mDhx58	GGAAGTGATCTTACCTGCTCTGG	TTGCCTCTGTCTACCGTCTCT
mIsg15	GGTGTCCGTGACTAACTCCAT	TGGAAAGGGTAAGACCGTCCT
mIrf7	GAGACTGGCTATTGGGGGAG	GACCGAAATGCTTCCAGGG
mUsp18	TTGGGCTCCTGAGGAAACC	CGATGTTGTGTAAACCAACCAGA
mOas1g	ATGGAGCACGGACTCAGGA	TCACACACGACATTGACGGC
mOas2	TTGAAGAGGAATACATGCGGAAG	GGGTCTGCATTACTGGCACTT
mOas3	TCTGGGGTCGCTAAACATCAC	GATGACGAGTTCGACATCGGT
mIl4	GGTCTCAACCCCCAGCTAGT	GCCGATGATCTCTCTCAAGTGAT
mIl13	CCTGGCTCTTGCTTGCCTT	GGTCTTGTGTGATGTTGCTCA
mTslp	ACGGATGGGGCTAACTTACAA	AGTCCTCGATTTGCTCGAACT
mIl33	CACTAAAATCGGGTACCAAGC	TGCTCTTGGTCTTTTCCAGAG
mIl1f9	TCCTGACTTTGGGGAGGTTTT	TCACGCTGACTGGGGTTACT
mCcl11	GAATCACCAACAACAGATGCAC	ATCCTGGACCCACTTCTTCTT
mCcl17	TACCATGAGGTCACTTCAGATGC	GCACTCTCGGCCTACATTGG
mCcl19	GGGGTGCTAATGATGCGGAA	CCTTAGTGTGGTGAACACAACA
mCcl22	AGGTCCCTATGGTGCCAATGT	CGGCAGGATTTTGAGGTCCA
mActb	GGCACCACACCTTCTACAATG	GGGGTGTTGAAGGTCTCAAAC

Supplementary Table 2. Antibody information

Antibody	Company	Catalog number	Application	Dilution fold
Rabbit anti-Ki67	Abcam	ab16667	IHC	1:200
Rabbit anti-Loricrin	Abcam	ab176322	IHC	1:250
Rabbit anti-Filaggrin	Abcam	ab81468	IHC	1:1000
Mouse anti- Cytokeratin 10	Abcam	ab76318	IHC	1:2500
Rabbit anti-Ly6g	Abcam	ab238132	IHC	1:2000
Mouse anti-dsRNA	Sigma-Aldrich	MABE1134-25UL	IHC	1:50
Brilliant Violet 510™ anti-mouse CD45	Biolegend	103137	Flow Cyt-IMQ	1:100
PerCP/Cyanine5.5 anti-mouse CD3	Biolegend	100218	Flow Cyt-IMQ	1:100
Alexa Fluor® 488 anti-mouse/human CD11b	Biolegend	101217	Flow Cyt-IMQ	1:100
APC anti-mouse CD11c	Biolegend	117309	Flow Cyt-IMQ	1:100
PE anti-mouse F4/80	Biolegend	123110	Flow Cyt-IMQ	1:100
APC anti-mouse CD45	Biolegend	103112	Flow Cyt-IMQ	1:100
PerCP/Cyanine5.5 anti-mouse CD90.2 (Thy-1.2)	Biolegend	140322	Flow Cyt-IMQ	1:100
PE anti-mouse TCR γ/δ	Biolegend	118108	Flow Cyt-IMQ	1:100
Brilliant Violet 605™ anti-mouse CD4	Biolegend	100548	Flow Cyt-IMQ	1:100
FITC anti-mouse CD8a	Biolegend	100706	Flow Cyt-IMQ	1:100
APC-Cyanine7 Anti-Mouse Ly6G (1A8)	Tonbo bioscience	25-1276-U100	Flow Cyt-IMQ	1:100
TruStain FcX™	Biolegend	101319	Flow Cyt-IMQ	1:50
Brilliant Violet 421™ anti-mouse CD45	Biolegend	103133	Flow Cyt-MC903	1:100
Alexa Fluor® 700 anti-mouse CD3	Biolegend	100216	Flow Cyt-MC903	1:100

Alexa Fluor® 488 anti-mouse/human CD11b	Biolegend	101219	Flow Cyt-MC903	1:100
Brilliant Violet 605™ anti-mouse Ly-6G/Ly-6C (Gr-1)	Biolegend	108439	Flow Cyt-MC903	1:100
APC anti-mouse CD11c	Biolegend	117309	Flow Cyt-MC903	1:100
Brilliant Violet 785™ anti-mouse CD326 (Ep-CAM)	Biolegend	118245	Flow Cyt-MC903	1:100
Brilliant Violet 650™ anti-mouse F4/80	Biolegend	123149	Flow Cyt-MC903	1:100
PerCP/Cyanine5.5 anti-mouse CD19	Biolegend	115533	Flow Cyt-MC903	1:100
PE anti-mouse FcεRIα	Biolegend	134307	Flow Cyt-MC903	1:100
PE/Dazzle™ 594 anti-mouse CD117 (c-kit)	Biolegend	135127	Flow Cyt-MC903	1:100
Zombie Aqua™ Fixable Viability Kit	Biolegend	423102	Flow Cyt-MC903	1:100